Simplified parameter extraction method for single and back-to-back Schottky diodes fabricated on silicon-on-insulator substrates

V. Mikhelashvili, R. Padmanabhan, and G. Eisenstein

Simplified parameter extraction method for single and back-to-back Schottky diodes fabricated on silicon-on-insulator substrates

V. Mikhelashvili,[1,2,a)] R. Padmanabhan,[1,2] and G. Eisenstein[1,2]
[1]*Electrical Engineering Department, Technion, Haifa 3200003, Israel*
[2]*Russell Berrie Nanotechnology Institute, Technion, Haifa 3200003, Israel*

We describe a technique to extract room temperature parameters of Schottky diodes based on single or double-terminal configurations whose barrier height is bias dependent. This method allows us to extract the zero bias barrier height without specific knowledge of interface states or the existence of insulator layers at the metal-semiconductor boundaries. This technique enables us to establish the type of thermionic emission mechanism, limited by a bias dependent image force potential and/or diffusion, taking into account interfacial states or layers. This technique makes use of experimental current-voltage (I-V) characteristics measured at both bias polarities and different intensities of illumination and the corresponding voltage-dependent differential slope-voltage characteristics $\alpha = dln(I)/dln(V)$. This method is verified experimentally on a conventional p-Silicon based Schottky diode and on metal-semiconductor and metal-insulator-semiconductor diodes fabricated on *n*-silicon-on-insulator substrates. Pd/Au Schottky electrodes were used, while the insulator stack of the metal-insulator-semiconductor diodes comprises an HfO_2 layer on top of an SiO_2 layer. *Published by AIP Publishing.* [http://dx.doi.org/10.1063/1.4994176]

I. INTRODUCTION

Numerous semiconductor devices and circuits make use of metal-semiconductor (MS) and metal-insulator-semiconductor (MIS) structures or their back-to-back (metal-semiconductor-metal (MSM) or MISM) configurations.[1] MS junctions exhibit either an Ohmic or a rectifying behavior; this is determined by the work-function of the metal (ψ_m), the electron affinity of the semiconductor (χ_S), the interfacial-trap density at the MS junction, the thickness of an interfacial layer (when such a layer exists), and the potential barrier. All these factors influence the barrier height, which is ideally the difference between the metal work function and electron affinity of the *n*-type semiconductor:[2] $\varphi_{bn} = \psi_m - \chi_S$, while for the p-type semiconductor, it is $\varphi_{bp} = E_g - (\psi_m - \chi_S)$, where E_g is the band gap of the semiconductor. The Ohmic or rectifying nature of a junction can be altered by a bias voltage, as well as illumination, temperature, and radiation. These external perturbations manifest themselves as a modification of the current-voltage (I-V) characteristics of the device. In the case where both electrodes form Schottky-type contacts in a MSM system, the carrier transport mechanism is complex; in particular, if the junctions are asymmetric (due to the use of electrode materials with different ψ_m values and or due to the presence of an interfacial insulator layer between the electrode and semiconductor[3]), double-Schottky MSM diodes and heterojunctions with different barrier heights are analysed as done in Refs. 4 and 5 by employing the thermionic emission theory model, which is valid for semiconductor substrates with doping levels, $N_{A,D}$, below $10^{17} cm^{-3}$.[6–8]

The influence of illumination on φ_{bn} and therefore on the photosensitivity of photodetectors was considered in Refs. 9–13. The reduction of φ_{bn} under illumination, in conjunction with the lowering of the potential barrier due to image-forces, was attributed to the change in the quasi-Fermi level in the semiconductor relative to the dark equilibrium state.[10] This was also used to explain the observed photosensitivity of I-V and capacitance-voltage (C-V) characteristics in MIS diodes.[2,14] Variations in different Schottky-barrier parameters also influence the photosensitivity of different MSM and MIS structures.[11–13] MIS structures with a leaky insulator stack containing many pores (metal seeping through the pores results in the formation of local MS junctions) were considered in Ref. 11. Under illumination, photogenerated holes are accumulated at the Si surface along the perimeter of the islands, enhancing the electric field around specific local points, thereby lowering φ_{bn}, which in turn increases the photosensitivity. The photocurrent intensification in MIS structures can also be attributed to edge fringing field effects.[12,13]

Most of the previously published papers[15–21] used graphical methods to extract parameters from forward biased I-V characteristics of Schottky diodes. All the extracted parameters, ideality factor, saturation current, and zero-bias barrier height (when the value of the linear series resistance is known), were assumed to be independent of the applied voltage. In Ref. 22, these parameters were extracted using the voltage difference of the differential slope (α–V, where $\alpha = \frac{d(lnI)}{d(lnV_R)}$) of I-V characteristics, additionally taking into consideration the non-linear series resistance and parallel conductance. A complex graphical differentiation of the experimental forward bias I-V characteristics was employed in Refs. 23 and 24 in order to extract the voltage-dependent ideality factor, after the extraction of surface states and traps in the interfacial layer between the Schottky electrode and semiconductor. Finally, Mikhelashvili *et al.*[25] analyzed the α–V characteristics, which enabled the extraction of the linear series resistance and voltage-dependent ideality factor

a)beso@ee.technion.ac.il

from the experimental I-V characteristics. However, this method assumes that the change in the image potential with applied voltage is linear, which is valid only at small biases.[26]

The strong influence of the barrier height on the characteristics of the devices comprising Schottky electrodes calls for a more effective method than those discussed above to evaluate the role of the electrode materials and geometry, as well as the effect of external perturbations. To this end, we have developed a comprehensive procedure, which in contrast to the previous studies allows establishing, from the reverse bias I-V characteristics, the most probable current flow mechanisms in a Schottky junction: thermionic emission limited or diffusion limited in the presence or absence of surface states at the metal-semiconductor boundary or without them in conjunction of an image force. Also determined are the image force potential and the zero voltage barrier height of holes (φ_{bp0}) or electrons (φ_{bn0}), as well as their modification with illumination. The method was verified for MS, MSM, and MISM structures with symmetric or asymmetric electrodes by the measurement of the current voltage characteristics (I-V) at room temperature under different illumination regimes. The developed method requires the knowledge of the doping level of the substrate only, with the assumption that surface states[1,26–28] with a constant density are monoenergetic or uniformly distributed in energy within the bandgap. For other types of distribution of interface states, it is essential to identify the distribution behavior.[29,30]

II. THEORETICAL ANALYSIS

The planar systems analyzed in this paper include pairs of diodes connected back-to-back via silicon. Systems comprising p-Si can be analyzed similarly. A simplified equivalent circuit of such a structure is shown in Fig. 1, where V_1 and V_2 are the voltage drops across diodes I and II, respectively. This model is based on the assumption that the voltage drop across Si can be neglected, when compared to the voltage drop across the reverse-biased diode junction, namely, the applied voltage equals $V = V_1 + V_2$. Based on the current continuity theory, the total current density $J_T = J_1 = J_2$ (for the system represented in Fig. 1) is given by[4,5]

$$J_T = \frac{2J_{s1}J_{s2}\sinh\left(\frac{qV}{2kT}\right)}{J_{s1}\exp\left(\frac{qV}{2kT}\right) + J_{s2}\exp\left(-\frac{qV}{2kT}\right)},\qquad(1)$$

where J_{s1} and J_{s2} are the leakage current densities through the reverse-biased Schottky junctions I and II, respectively; T, q, and k are the absolute temperature, electron charge, and
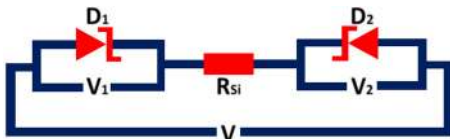

FIG. 1. The schematic electrical circuit of a back-to-back connected pair of diodes (R_{Si} is the Si layer resistance).

Boltzmann constant, respectively, while current density $J = \frac{I}{S}$, where S is the electrode area.

One of the diodes I or II is always reverse biased and hence limits the net current for either bias polarity. J_{s1} and J_{s2} at reverse-biased Schottky junctions with unequal barrier heights are given as follows:[1,27,28]

$$J_{s1},\, J_{s2} = \frac{\theta q N_{v,c} v_R \exp\left(-\frac{q\varphi_{bp1,n1},\, q\varphi_{bp2,n2}}{kT}\right)}{\left(1 - \frac{\theta v_R}{v_D}\right)},\qquad(2)$$

where $\varphi_{bp1,n1}$ and $\varphi_{bp2,n2}$ are the voltage-dependent barrier heights at the junctions I and II, respectively; v_R and v_D are the thermal and effective diffusion velocities of carriers, respectively; N_v and N_c are the effective density of states in the valence or conduction bands, respectively; and θ is the barrier transmission coefficient ($\theta < 1$ or $\theta = 1$, for barriers with or without an interfacial layer, respectively). The relation between thermal and effective carrier diffusion velocities determines the role of the thermionic emission or diffusion current flow mechanisms.

Leakage current density in an ideal Schottky diode is independent of the applied reverse-bias; it is determined only by $\varphi_{bp,n} = \varphi_{bp0,n0}$. However, real Schottky diodes exhibit a significant increase in leakage current with reverse bias due to the voltage-dependence of the Schottky barrier height. The increase in leakage current is larger than that caused by thermally-generated minority carriers within the expanding depletion region. The Schottky barrier height is reduced in the dark due to both a variation of image force potential and a dipole layer, which results from an interfacial layer with surface trap states and or fixed charges at the MS boundary.[1,27,28] The barrier height reduces further under illumination[10]

The variation of $q\varphi_{bn}$ is generally expressed as[9,27,28]

$$\varphi_{bp1,n1},\, \varphi_{bp2,n2} = \varphi_{bp01,n01},\, \varphi_{bp02,n02} \pm \Delta\varphi,\qquad(3)$$

where

$$\Delta\varphi = \left(1 - \frac{1}{n_0}\right)V_R + \Delta\varphi_0 + \Delta\varphi^{ill}.\qquad(4)$$

The interfacial layer, image force, and illumination related contributions are denoted as

$$\frac{1}{n_0} = \frac{\varepsilon_0\varepsilon_i}{\varepsilon_0\varepsilon_i + q^2 d_i D_{it}},\qquad(5)$$

$$\Delta\varphi_0 = \left(\frac{q^3 N_{A,D}}{8\pi^2\varepsilon_o^3\varepsilon_s^3}\right)^{1/4}\left[\left(V_{bi} + |V_R| - \frac{kT}{q}\right)^{1/4}\right],\qquad(6)$$

and

$$\Delta\varphi^{ill} = (E_{fn}^{ill} - E_f) \quad \text{or} \quad \Delta\varphi^{ill} = (E_f - E_{fp}^{ill}),\qquad(7)$$

respectively, for n- and p-type semiconductors.

The $\pm$ sign in (3) denotes forward bias (V_F) and reverse (V_R) bias, respectively. ε_0, ε_i, and d_i are the free space permittivity, dielectric constant, and thickness of the interfacial

layer, respectively, while D_{it} is the density of the surface states per unit energy and area. Surface states are assumed to be uniformly distributed in energy within the bandgap. $V_{bi} = \psi_s - \psi_m + \frac{kT}{q}\ln\left(\frac{N_v}{N_A}\right)$ and $V_{bi} = \psi_m - \psi_s - \frac{kT}{q}\ln\left(\frac{N_c}{N_D}\right)$, where N_A and N_D are the built-in voltages (or diffusion potentials) and the acceptor donor concentration, respectively, of p- or n-type semiconductors; and ψ_s is the work function of the semiconductor. $\varphi_{bn01}, \varphi_{bn02} = (\psi_{m1}, \psi_{m2} - \chi_s)$ are the barrier heights at zero bias; ψ_{m1} and ψ_{m2} are the work functions of the metal electrodes. The corresponding hole barrier heights are $\varphi_{bp01}, \varphi_{bp02} = \frac{1}{2}E_g - (\psi_{m1}, \psi_{m2} - \chi_s)$, where E_g is the semiconductor band gap. E_F, E_{fn}^{ill}, and E_{fp}^{ill} are the equilibrium Fermi and quasi Fermi levels of electrons or holes under illumination, while $(E_{fn}^{ill} - E_f) = kTLn\left(\frac{n_i^{ill}}{N_D}\right)$ and $(E_f - E_{fp}^{ill}) = kTLn\left(\frac{n_i^{ill}}{N_A}\right)$, with n_i^{ill} the illumination intensity dependent intrinsic carrier concentration.[10]

At small D_{it} values, when $\varepsilon_o\varepsilon_i \ll q^2 d_i D_{it}$ [see Eq. (5)], the barrier height changes by the image force. The relationship between thermal and diffusion velocities distinguishes between two limiting Schottky current mechanisms in MSM or MIS structures. When $\theta v_R \ll v_D$ [see Eq. (2)], only thermionic emission determines the current flow, while for large θv_R values, carrier diffusion from the edge of the depletion layer to the peak of the image force potential (electrostatic potential of the conduction band) limits the current. Inserting Eqs. (3) and (4) into (2) leads to several current transport mechanisms that take place in real Schottky diodes and therefore in pairs of back-to-back connected devices. The thermionic and diffusion mechanisms in reverse biased Schottky diodes (taking into account an interfacial layer and the transmission coefficient of the barrier to be smaller than unity[27,28]) are approximated by

$$J_{s,thermionic} = \theta A^* T^2 \exp\left(-\frac{q\varphi_{bp0,n0}}{kT}\right)\exp\left(\frac{q\Delta\varphi}{kT}\right), \quad (8)$$

$$J_{s,diffusion} = q\mu N_{v,c}\left(\frac{2qN_{A,D}}{\varepsilon_0\varepsilon_s}\right)^{\frac{1}{2}}(V_{bi} - V_R)^{\frac{1}{2}}$$
$$\times \exp\left(-\frac{q\varphi_{bp0,n0}}{kT}\right)\exp\left(\frac{q\Delta\varphi}{kT}\right), \quad (9)$$

where A^* is the effective Richardson constant (for n-Si, $A^* = 120m^*_e$, with m^*_e being the effective mass of the electron). Based on Eqs. (3)–(6), we propose a simple analytical method to analyze experimental current-voltage characteristics in order to discriminate among the carrier transport mechanisms (thermionic or diffusion with or without the influence of an interfacial layer) and to extract the zero bias Schottky barrier height and the voltage dependence of the image force.

We analyze the α-V curves, whose usefulness in the extraction of the diode parameters was demonstrated in Refs. 22, 25, and 31–36. The technique we propose does not require to resort to complicated graphical differentiation techniques as given in Refs. 23 and 24 for the extraction of bias-dependent parameters, and it is unlike the technique reported in Ref. 37, which is only valid under limited conditions.

Simple algebraic manipulation of Eqs. (8) and (9) yields two pairs (for the thermionic and diffusion cases) of analytical expressions of α-V_R in order to extract the values of voltage dependent lowering of the barrier height (with or without interfacial states influence). These equations are summarized in Table I.

The behavior of the calculated reverse I-V_R and α–V_R characteristics in all the particular cases considered above is summered in Fig. 2. As predicted by Eq. (1), the total current in back-to-back connected diodes is limited by the reverse biased diode, while the influence of the forward direction biased diode is insignificant due to its low differential resistance.

The I-V_R characteristics of structures with equal ($\varphi_{bn01} = \varphi_{bn02} = 0.8\,\text{eV}$) and unequal ($\varphi_{bn01} = 0.8\,\text{eV}$ and $\varphi_{bn02} = 0.73\,\text{eV}$) barrier heights reveal symmetric and asymmetric

TABLE I. Extraction of the exponential coefficient [Eqs. (8) and (9)] bias dependent $\Delta\varphi$ at different current flow mechanisms of the thermionic emission.

| Conditions	Current flow mechanisms	$\alpha - V_R$ dependence	$\Delta\varphi$, eV
Without interfacial layer or states	Thermionic limited current, taking into account image force potential ($\theta v_R \ll v_D$)	$\alpha = \frac{qV_R}{kT}\frac{d(\Delta\varphi)}{dV_R}$	$\frac{kT}{q}\int_{V_R=0}^{V_R}\frac{\alpha}{V_R}dV_R + C_1$ $\Delta\varphi = \Delta\varphi_0$ (10)
Without interfacial layer or states	Diffusion limited thermionic current ($\theta v_R \gg v_D$)	$\alpha = \dfrac{\frac{qV_R}{kT}\frac{d(\Delta\varphi_0)}{dV_R}}{-\frac{1}{2}\frac{V_R}{(V_{bi}-V_R)}}$	$\frac{kT}{q}\left\{\left[\int_{V_R=0}^{V_R}\frac{\alpha}{V_R}dV_R - \frac{1}{2}\ln(|V_{bi}-V_R|)\right]\right\} + C_1 + C_2$ $\Delta\varphi = \Delta\varphi_0$ (11)
With interfacial layer or states	Thermionic limited current ($\theta v_R \ll v_D$)	$\alpha = \frac{qV_R}{kT}\frac{d(\Delta\varphi)}{dV_R}$	$\frac{kT}{q}\int_{V_R=0}^{V_R}\frac{\alpha}{V_R}dV_R + C_1$ $\Delta\varphi = \left(1 - \frac{1}{n_0}\right)V_R + \Delta\varphi_0$ (12)
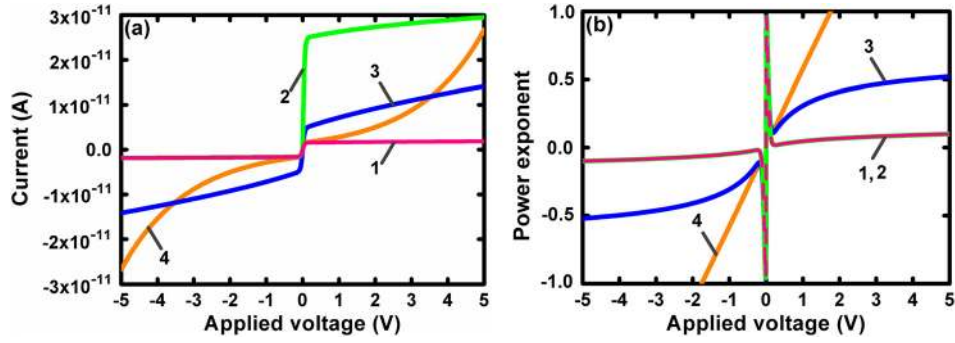
FIG. 2. (a) Current-voltage and (b) α-V characteristics of the back-to-back connected MS diodes simulated in accordance with Eq. (1) for different current flow mechanisms descripted by Eqs. (8) and (9). The equal and different zero biased barrier heights for curves 1 and 2-thermionic emission limited current are $\varphi_{bn01} = \varphi_{bn02} = 0.8$ eV and $\varphi_{bn01} = 0.73$ eV and $\varphi_{bn02} = 0.8$ eV, respectively; for curves 3 and 4 in the cases of diffusion limited current and thermionic limited current at availability of the interfacial layer or states, respectively, the equal barrier height is $\varphi_{bn01} = \varphi_{bn02} = 0.8$ eV. The rest calculation parameters are $A^* = 120 m_e^*$ A cm^{-2}K^{-2}, T $= 300$ K, $N_D = 8 \times 10^{13}$ cm^{-3}, $N_c = 2.8 \times 10^{19}$ cm^{-3}, $\theta = 1$, $V_{bi} = 0.82$ eV, $\varepsilon_s = 11.8$, $\mu = 1400$ cm^2 V^{-1}s^{-1}, $D_{it} = 1 \times 10^{11}$ cm^{-2}eV^{-1}, $d_i = 3$ nm, and $S = 3.4 \times 10^{-6}$ cm^2.

characteristics (see curves 1 and 2) in Fig. 2(a), respectively. Curves 1 and 2 were calculated considering the thermionic emission limited case and lowering of the barrier height only by the voltage dependent image force. The consequent α–V_R characteristics [Fig. 2(b)] are symmetric in both cases independent of the barrier height difference. The reason is that the differential slope value and its change with applied reverse voltage are determined only by the variation of the image force potential. When the diffusion limited current dominates, for equal zero biased barrier heights, the total current is more than one order of magnitude larger than in the thermionic emission case. The dependence of the pre-exponential term on applied reverse voltage [see Eq. (9)] causes the differential slope to change fast with applied bias as compared to the thermionic emission case. The transition regions in both current flow mechanisms are almost linear (α values at zero bias approach 1). The I-V_R curves were calculated next for diodes, which include thin interfacial layers at the metal semiconductor interfaces. The calculation assumed again equal barrier heights. The voltage dependence of the reverse current on applied voltage is symmetric once more but with larger values that increase exponentially with bias. This also exhibited in the α–V_R behavior [see curve 4 in Fig. 2(b)], which is linear with applied voltage, in contrast to cases without an interfacial layer and also depends strongly on the density of the interface states.

Solving numerically the two equation system that includes Eq. (4) and the expression of the differential slope

$$\alpha = \frac{|V_R|}{kT}\left[\left(1 - \frac{1}{n_o}\right) - \frac{d\Delta\varphi_o}{dV_R}\right], \tag{13a}$$

$$\frac{d\Delta\varphi_o}{dV_R} = \frac{1}{4}\left(\frac{q^3 N_{A,D}}{8\pi^2\varepsilon_o^3\varepsilon_s^3}\right)^{1/4}\frac{1}{\left(V_{bi} + |V_R| - \frac{kT}{q}\right)^{3/4}} \tag{13b}$$

enables us to estimate the values of $\left(1 - \frac{1}{n_o}\right)$ from experimental data and hence D_{it} used in Eq. (5). Equation (13a) is obtained from Eq. (8), taking into account that $\Delta\varphi$ in (4) is affected by interfacial states and the image force potential as in Eqs. (5) and (6).

The value of $\Delta\varphi$ extracted from experimental I-V_R and α–V_R characteristics in accordance with the proper equations of the table enables the calculation of the zero biased barrier height from Eqs. (8) or (9)

$$\varphi_{bp0,n0} = kTln\left(\frac{I}{AS}\right) - \Delta\varphi, \tag{14}$$

where I and A are the measured total current and the pre-exponential multiplier in (8) and (9), respectively. There are several difficulties in establishing accurately the contact parameters in the case where a thin insulator layer exists between the metal and the semiconductor. The difficulties stem from the fact that the measured leakage current is sensitive to local non-uniformities (non-uniform thickness, crystalline inclusions embedded into the amorphous matrix, or grain boundaries). In addition, when the films are subjected to a high electric field, injection into an insulator may modify the insulating properties permanently even in the absence of local non-uniformities. This makes it impossible to determine the actual electrode area contacting non-uniform current channels, which actually defines the measured current density and therefore the Schottky barrier height in accordance with Eq. (14). The transmission coefficient, which is usually assumed to be about 1, may reduce from this ideal value under large electric fields ($\gg 1$ MV/cm) due to the auto electron emission phenomenon.[8,38] Note that the image force potential value is not a function of the real area of the electrodes and transmission coefficient. Thus, the method allows us to establish the value and the trend of the barrier height dependence on illumination with satisfactory accuracy.

III. EXPERIMENTAL VERIFICATION

The parameter extraction technique and discrimination among transport mechanisms were employed in three different Schottky devices: a commercial n-Si Schottky diode (MA40147-213) and two experimental planar structures fabricated on Silicon-on-Insulator (SOI) substrates, one being a symmetric back-to-back connected metal-semiconductor-metal (MSM) structure and the second a metal-insulator-semiconductor-metal (MIS-MS) diode which is asymmetric.

The SOI substrate included a 3 μm thick n-Si device layer with a resistivity of 50 Ωcm and a 1.4 μm thick SiO$_2$ box layer. The MSM and MIS-MS structures are comprised of similar electrodes: an electron beam gun evaporated Pd/Au stack, which ensured a high potential barrier, and the insulator stack, which included a 3 nm thermal SiO$_2$ layer covered by an atomic layer deposited 20 nm HfO$_2$ film. Pt nanoparticles grown *in-situ* with the HfO$_2$ film were embedded between the two insulator layers. The measurement of the SOI based devices was carried out in the dark and under illumination at 365 nm. The optical signal was applied via a fiber lens. The electrode area in the MSM diode was 1.6 $\times 10^{-5}$ cm^2 with an inter electrode distance of 20 μm, which was illuminated uniformly with a spot area of 1.7×10^{-6} cm^2. In the MIS-MS structure, only the MIS branch was illuminated. In order to ensure the asymmetric illumination, the interelectrode distance was increased to 135 μm where the electrodes were connected via the silicon device layer. The electrode area in the MIS diode was 1.75×10^{-6} cm^2. A schematic image of the measured structure is similar to that described in Ref. 3.

The MIS-MS structure underwent a voltage stress process[14] in order to form filament paths, which enable a leakage path for the photocurrent. All the experiments were conducted for a variable gate voltage and a grounded back electrode. The I-V characteristics were measured at room temperature using an Agilent 4155C Semiconductor parameter analyzer.

A. Single Schottky diode

Measured I-V characteristics of a commercial Schottky diode and the corresponding calculated α-V characteristics are shown by solid lines in Figs. 3(a) and 3(b). The typical exponential behavior at forward bias and saturation under reverse bias conditions are clearly observed. The more sensitive α-V dependences reveal a very small α value in the range of 0.08–0.11 [see the inset in Fig. 3(b)] under reverse bias, while in the forward bias case, α is larger than 1 over a limited voltage range and eventually reaches a peak when the current is limited by the MS junction barriers. At this point, the current flow mechanism changes from exponential to one that is dominated by the series resistance of the bulk semiconductor and the Ohmic back contact.

The parameters of the maximum point (α_{max}, V_{max}, and I_{max}) enable the extraction of the ideality factor, total barrier height φ_{bn}, and series resistance,[22] which in the present case are 1.12, 0.65 eV, and 0.89 Ω, respectively, under the assumption that these parameters are voltage-independent. An ideality factor value of about 1.12 was estimated from the maximum of the α-V plot in accordance with the method described in Ref. 22, which assumes the Schottky barrier height to be independent of the applied voltage. Therefore, the extracted ideality factor value is an approximate one. The real voltage dependence of the ideality factor, in accordance with Refs. 1 and 26, is expressed as $n \approx 1/(1 - \frac{d\Delta\varphi}{dV})$, assuming the voltage independent Richardson coefficient. A correct curve depicting the dependence of the ideality factor with applied bias is shown in Fig. 3(d), which takes the voltage-dependence of the extracted image force potential into account [see Fig. 3(c)]. It is seen that n reduces from 1.027 at $V > 0.05$ V to 1.005 at $V = 0.4$ V. Therefore, the small deviation of the ideality factor from a value of unity indicates that the current flow by thermionic emission is disturbed by the effect of the voltage dependent image force potential.[1,26] A similar procedure can be used to establish the
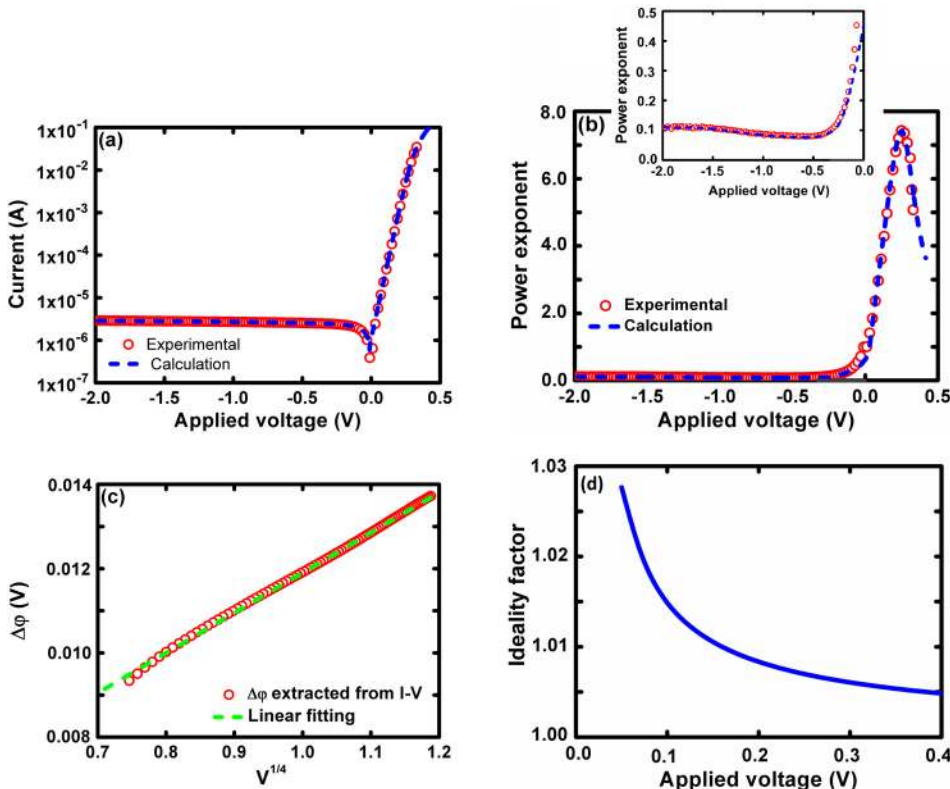

FIG. 3. Experimental (symbols) and calculated (dashed lines) (a) current-voltage and (b) α-V characteristics of a single Schottky diode measured in the dark regime. The inset shows the α-V dependence in an enlarged scale. (c) Extracted image force potential versus $V_R^{1/4}$ (symbols) and linear fit curves (dashed line). (d) Extracted ideality factor versus applied voltage.

behavior of the ideality factor with applied bias in the common case [see Eq. (4)] when interfacial states are present with or without incorporation of the image force potential. This is further proven by the weak dependence of α on the reverse bias. Moreover, $\alpha \ll 0.5$ (at reverse bias) indicates that diffusion limited thermionic emission (which is characterized by $\alpha \approx 0.5$) does not take place. In addition, interfacial states (or a thin interfacial insulator layer) at the metal-semiconductor interface are also absent since α does not depend linearly on the applied voltage. Further evidence lies in the linear dependence on $V_R^{1/4}$ of the $\Delta\varphi$ value, extracted by from Eq. (10) shown in Table I and Fig. 3(c). This indicates that the thermionic emission mechanism with voltage modified image force potential dominates [see Eq. (6)]. The zero bias barrier height, estimated by Eq. (14), taking into consideration Eq. (4), is 0.64 eV. It differs from the value obtained from the forward bias I-V characteristics, which is the sum of $\varphi_{bno} + \Delta\varphi_o$ [see Eq. (3)] and takes the value of 0.65 eV. The calculated I-V and α–V curves (which use the extracted parameters, when $\theta = 1$) are plotted in Figs. 3(a) and 3(b) as dashed lines. The inset shows the reverse bias portion of the α–V plot, in a magnified scale. The perfect coincidence testifies to the strength of the proposed method, which is simpler than the complicated current versus

temperature technique of extraction of the zero bias barrier height of single Schottky diodes.[1]

B. Back-to-back connected structure with symmetric Schottky electrodes

Next, we examine the proposed technique for MSM diodes operating in the dark and under illumination. Experimental I-V and α–V curves are shown in Figs. 4(a) and 4(b), respectively.

As predicted by Eqs. (1) and (2) [see Fig. 2(b)], the I-V characteristics are saturated for both bias polarities for $|V| > 0.8$ V. For bias levels smaller than 0.8 V and independent of illumination, α increases as the bias is reduced and at $|V|=0$ V it reaches unity.

A qualitative analysis of the experimental α–V characteristics indicates that it is consistent with the theoretical curves shown in Fig. 2(b) (α measured in the dark is approximately 0.45). At large voltages, α saturates with the average value reducing from 0.45 in the dark to 0.2 within a small range of illumination intensities of less than 4×10^{-8} W. In the illumination range of 4×10^{-8} W to 2.5×10^{-6} W, α varies in the small range of 0.1–0.2. We conclude that under low illumination, the current flow mechanism is close to
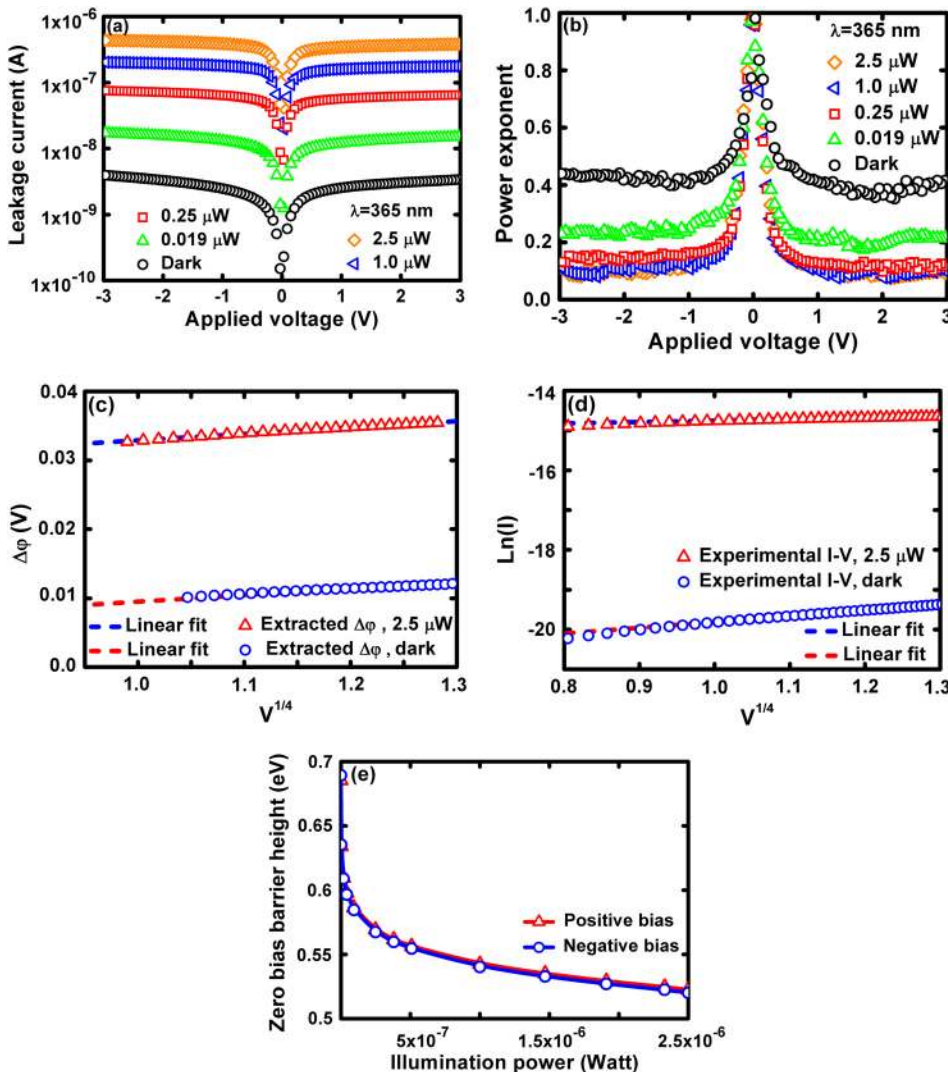

FIG. 4. A set of experimental (a) current-voltage and (b) differential slope-voltage characteristics of a planar MSM structure with symmetric metallic electrodes, measured in the dark and under illumination. (c) Image force potential extracted from experimental data. (d) Logarithm of the experimental current dependences on $V_R^{1/4}$ and the linear fit in the dark and under illumination powers of 2.5×10^{-6} W. (e) Zero bias barrier height versus illumination power extracted from I-V and α–V at both bias polarities.

diffusion-limited thermionic emission (where $\alpha \sim 0.45$ which is close to the theoretical of 0.5) with the incorporation of bias dependent image force potential. However, increasing the illumination intensity leads to thermionic emission, which is limited only by the barrier height variation due to image force potential changes with applied voltage. The measured sub-linear character of $\alpha - V$ for all bias levels precludes any role of interfacial states or an interfacial layer at the metal-semiconductor interfaces similar to that observed for the single Schottky diode discussed above. The reason is that interfacial states would lead to an exponential dependence of the reverse saturation current on applied voltage and therefore a linear increase in α with applied voltage, as predicted by Eqs. (2) or (8) taking into consideration (3) and (4).

Figures 4(c) and 4(d) present extracted $\Delta\varphi$ and experimental $Ln(I)$ versus $V_R^{1/4}$ in the dark and illumination regimes. The linear character of the curves indicates that only variations of the image force potential with applied bias limit the voltage dependence of the exponential part of the I-V characteristic, in accordance with Eqs. (6) and (8).

$\Delta\varphi = \Delta\varphi_o$ calculated from the experimental I-V and α–V curves, using the equations given in Table I, increases with illumination [see Fig. 4(c)] but maintains the linear $V_R^{1/4}$ dependence similar to the dark regime. In the dark and at small illumination powers, $\Delta\varphi_o$ values were extracted by Eq. (11) in Table I, while at large illuminations, we used Eq. (10). This causes a reduction of the zero biased dark barrier height in both bias polarities from 0.68 eV to 0.525 eV. The illumination power dependences of the zero bias barrier heights, calculated for both bias polarities with and without diffusion limited thermionic emission regimes, are shown in Fig. 4(e). As expected, the dependencies are similar due to the identical metallic stack used in both electrodes. The small difference in the extracted curves is due to deviations from the uniform illumination of the interelectrodes area.

The enhancement of the thermionic emission of carriers into the semiconductor under illumination due to lowering of the barrier height was discussed in Refs. 9, 39, and 40. Illumination induces a difference between the quasi-Fermi level of the photo-excited holes in the depletion region of an n-type semiconductor and the equilibrium Fermi level.

Under illumination, the full reduction of the barrier height should be considered in Eqs. (4) and (7).

Figures 5(a) and 5(b) compare the experimental (symbols) and calculated (dashed lines) I-V and α–V curves, in the dark and under maximum illumination. The curves were calculated according to Eqs. (9) and (14) using the extracted parameters from the experimental I-V characteristics. The agreement between calculated and experimental curves, especially in the saturation regime, as well as their similar behavior to the simulated results of Fig. 2, is quite remarkable. Finally, we note that the measured symmetrical I-V and α-V characteristics with zero photo current at zero bias is due to the zero electric field at the center of the potential well caused by the two identical rectifying electrodes. This is in contrast to the single Schottky photodiode where at zero bias, the internal electric field formed by the work function difference between metal-semiconductors induces a finite photocurrent.[1]

C. Back-to-back connected MIS and MS structures with asymmetric junctions and illumination

I-V characteristics of a MIS-MS structure measured are shown in Fig. 6(a). The illumination was non-uniform: the MIS part of the device was illuminated, while the MS section was in the dark regime.

The first difference from the MSM data [see Figs. 4(a) and 4(b)] is [see Figs. 6(a) and 6(b)] that at negative bias, conventional photocurrent with illumination is observed, while at positive bias, it is significantly lower although it is higher than the dark current. The effect of illumination on the MS junction current (which is in the dark) is due to drift-diffusion via the Si layer of the photogenerated minority carriers from the positive biased illuminated gate area, while MS junction is under negative polarity of the voltage.[41] Minority carriers that accumulate at the MS interface attract majority carriers from the reverse biased electrode and hence cause an increase in the net current.[2]

The second difference is that under illumination and negative bias, the I-V curve changes super linearly. This is clearly seen in Fig. 6(b) (see the inset with curves enlarged along the voltage scale), where the α-V curves, measured in
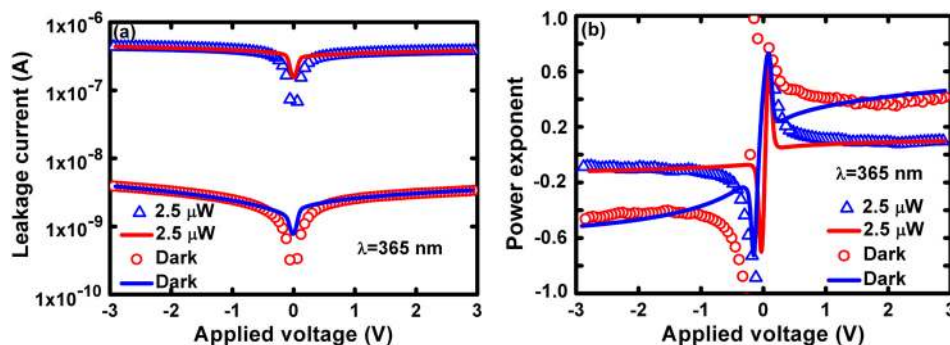

FIG. 5. Experimental (symbols) and calculated (solid lines) (a) current-voltage and (b) differential slope-voltage characteristics of the MSM structures measured in the dark and under illumination at 2.5×10^{-6} W. Calculation in the dark regime and under illumination considered the extracted image force potential assuming thermionic emission with and without limitations by diffusion and the absence of interfacial states or layers. In the calculation, the extracted values of φ_{bn0} equal to 0.69 eV in the dark and 0.525 eV under illumination were used. The other parameters of calculation in Eqs. (2), (8), and (9) are $\theta = 1$, $A^* = 120 m^*$ A cm^{-2}K^{-2}, and T = 300 K.
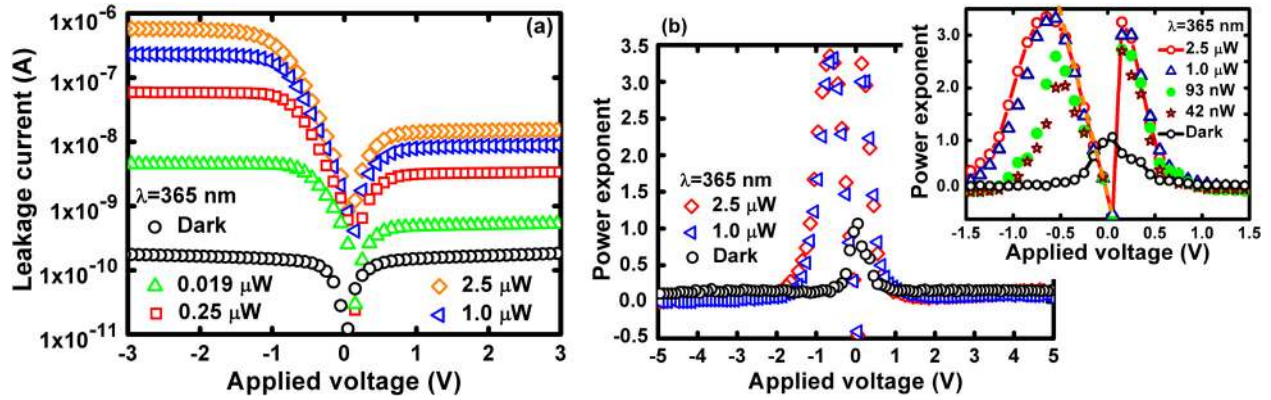
FIG. 6. The experimental (a) current-voltage and (b) differential slope-voltage characteristics of a planar MISM structure on a SOI substrate with identical metallic electrodes, measured in the dark regime and under illumination. The inset shows the part of the α-V curves measured at small voltages, while the dashed line indicates a linear fit.

the dark and under illumination, reach large values in the vicinity of zero bias. For positive bias, the behavior is similar to that of the MSM structure [see Fig. 4(b)]. The α-V curves under illumination are linear and in the bias range of 0 V to −0.65 V [see the linear fit in the inset of Fig. 6(b)], while for −1.5 V to −5 V, they are sublinear. For both bias polarities in the dark regime and for positive bias under illumination, a region with $\alpha \ll 0.5$ is observed similar to the MSM structure [see Fig. 4(b)].

We postulate that the reason for the change in the nature of the contact from rectifying (where $\alpha \ll 1$) under reverse bias and in the dark to injecting (with $\alpha > 1$) under illumination is the accumulation of photogenerated minority carriers at the semiconductor surface, which attract majority carriers from the gate electrodes so as to ensure charge neutrality across the junction. The almost linear character of α-V [see the inset in Fig. 6(b)] is due to the contribution of interfacial traps in the thermionic emission process, in accordance with Eq. (4). This however cannot explain the revelation of a maximum point in the α-V curves. The super linearity of the I-V characteristics can also be induced by the space charge limited current due to filling of interfacial or bulk traps originating from the filamentation process and the Pt NPs. In the low voltage range, the gate electrode has a limited capacity to supply external carriers; the drop of the α-V curve following the maximum can only be induced by such a change in the capability of the electrode to supply excess carriers. In accordance with Refs. 7,42, and 43, when the current is sufficiently high or when the electric field at the metal-semiconductor interface gap is large, the real value of the effective contact concentration formed close to the semiconductor surface decreases, and therefore, the character of the current flow mechanism changes from limited by traps to the Schottky barrier height. All these effects result in a non-monotonic α-V curve seen in Fig. 6. Enhancement due to the illumination of the local electric fields in MIS structures with ultrathin porous insulators compared to uniform films was discussed in Ref. 11, while a similar effect due to edge fringing fields in the vicinity of the electrodes was considered in Refs. 11–13. A comparable increase in the local electric field in the filament regions of the insulator stack is

expected at negative voltages ($|V|>1.5$ V), corresponding to the saturation region of the I-V characteristics ($\alpha<1$).

It is seen in Fig. 6(b) that in the dark regime, the reduction and saturation of α in both bias polarities are observed immediately after the maximum at $\alpha \cong 1$ [analogous to the curves in Figs. 2(b) or 5(b)] in a very small voltage range close to zero. The explanation is that the bulk carrier concentration in the Si layer is not perturbated by the externally injected carriers, whose density is limited by the large barrier height, and they are exclusively captured by interfacial traps. The reason for the weak voltage dependence of the current and therefore the small values of α in both bias polarities is analogous to the MSM case where the image force potential affects the barrier height.

At negative bias on the MS part of the device, the influence of illumination and interfacial layer is negligible, and hence, α–V behaves analogous to the MSM structure or the dark regime. The maximum α-V value at very small bias [see the inset in Fig. 6(b)] is not due to the interfacial states at the MS boundary but rather due to a change in the sign of the current at the inflection point close to zero bias. Finally, the diffusion mechanism is excluded as the α at any applied bias differs significantly from the theoretical value of 0.5.

Figure 7 describes the influence of illumination power on the lowering of the barrier height in both junctions: MIS and MS. At any illumination power, the determination of the
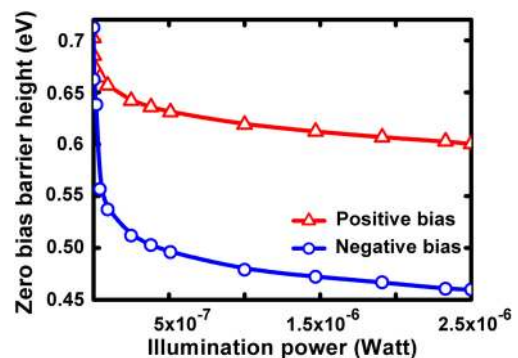

FIG. 7. The dependence of the zero bias barrier height on illumination power in the case of an asymmetric illumination of the branches of the MISM structure.

zero bias barrier height at negative bias assumes that two factors determine the exponential factor: the presence of interfacial states and an image force potential. Therefore, using experimental I-V and α-V curves and the procedure given in Eq. (12) of Table I, we extract $\Delta\varphi$ [see Eq. (4)] and hence the barrier height. At positive bias, the voltage dependence of the barrier height is only limited by the image force potential (see Eq. (10) in Table I). Figure 7 clearly demonstrates the effect of the non-uniform illumination on the asymmetric variation of the barrier heights in the gate and back electrodes, as the net current is different in different branches (MIS and MS). In the dark, the zero bias barrier heights are almost identical, which are about 0.7 eV and 0.71 eV. However, a significant deviation in the zero bias barrier height is already clearly observed at small illumination powers of about 1.0×10^{-9} W.

IV. CONCLUSIONS

We presented a new method for the extraction of the zero bias barrier height and for the reproduction of the image force potential dependence on voltage of single and back-to-back connected Schottky structures, from experimental I-V characteristics. The translation of the I-V characteristics to the voltage dependent differential slope curve establishes the dominant thermionic emission mechanisms among alternative ones (limited by diffusion, bias varied image force potential, interfacial states, or their combinations). We show a successful fitting of the current-voltage dependences of different structures by parameters extracted from experimental I-V curves measured at different illumination regimes. The advantage of the proposed technique over other published methods[1,5,40] is the zero bias barrier height of Schottky diodes used in single or back-to-back configurations without assuming that interfacial states or insulator layer exist, even at room temperature.

[1]S. M. Sze and K. K. Ng, *Physics of Semiconductor Devices* (John Wiley and Sons, New York, 2006).

[2]N. F. Mott, Proc. Camb. Philos. Soc. **34**, 568 (1938).

[3]V. Mikhelashvili, R. Padmanabhan, B. Meyler, S. Yofis, and G. Eisenstein, J. Appl. Phys. **120**, 224502 (2016).

[4]X.-L. Tang, H.-W. Zhang, H. Su, and Z.-Y. Zhong, Physica E **31**, 103 (2006).

[5]A. J. Chiquito, C. A. Amorim, O. M. Berengue, L. S. Araujo, E. P. Bernardo, and E. R. Leite, J. Phys.: Condens. Matter **24**, 225303 (2012).

[6]C. R. Crowell and S. Sze, Solid State Electron. **8**, 1035 (1966).

[7]F. A. Padovani, Solid State Electron. **12**, 135 (1969).

[8]A. N. Zyuganov and S. V. Svechnikov, *Injection Contact Phenomena in Semiconductors* (Naukova Dumka, Kiev, 1981).

[9]T. Y. Chen and J. G. Hwu, ECS J. Solid State Sci. Technol. **3**, Q37 (2014).

[10]Q. Yang, X. Guo, W. Wang, Y. Zhang, S. Xu, D. H. Lien, and Z. L. Wang, ASC Nano **4**, 6285 (2010).

[11]O. Malik, V. Grimalsky, and J. De La Hidalga-W, Sens. Actuators, A **130**, 208 (2006).

[12]C. Y. Yang and J. G. Hwu, IEEE Sens. J. **12**, 2313 (2012).

[13]T. Y. Chen and J. G. Hwu, Appl. Phys. Lett. **101**, 073506 (2012).

[14]V. Mikhelashvili, D. Cristea, B. Meyler, S. Yofis, Y. Shneider, and G. Atiya, J. Appl. Phys. **116**, 074513 (2014).

[15]H. Norde, J. Appl. Phys. **50**, 5052 (1979).

[16]C. D. Lien, F. C. T. So, and M. A. Nicolet, IEEE Trans. Electron Devices **ED-31**, 1502 (1984).

[17]S. K. Cheung and N. W. Cheung, Appl. Phys. Lett. **49**, 85 (1986).

[18]J. H. Werner, Appl. Phys. A: Solids Surf. **47**, 291 (1988).

[19]T. C. Lee, S. Fung, C. D. Beiling, and H. L. Au, J. Appl. Phys. **72**, 4739 (1992).

[20]D. Gromov and V. Pugachevich, Appl. Phys. A: Solids Surf. **59**, 331 (1994).

[21]V. Aubry and F. Meyer, J. Appl. Phys. **76**, 7973 (1994).

[22]V. Mikhelashvili, G. Eisenstein, V. Garber, S. Fainleib, G. Bahir, and D. Ritter, J. Appl. Phys. **85**, 6873 (1999).

[23]K. Maeda, H. Ikoma, K. Sato, and T. Ishida, Appl. Phys. Lett. **62**, 2560 (1993).

[24]T. Ishida and H. Ikoma, J. Appl. Phys. **74**, 3977 (1993).

[25]V. Mikhelashvili, G. Eisenstein, and R. Uzdin, Solid-State Electron. **45**, 143 (2001).

[26]E. H. Rhoderick and R. H. Williams, *Metal–Semiconductor Contacts* (Oxford University Press, USA, 1988).

[27]C.-Y. Wu, J. Appl. Phys. **51**, 3786 (1980).

[28]C.-Y. Wu, J. Appl. Phys. **53**, 5947 (1982).

[29]E. H. Nicolian and J. R. Brews, *MOS Physics and Technology* (John Wiley, New York, 1982).

[30]C. Barret and A. Vapaille, Solid State Electron. **18**, 25 (1975).

[31]V. Mikhaelashvili, Y. Betzer, I. Prudnikov, M. Orenstein, D. Ritter, and G. Eisenstein, J. Appl. Phys. **84**, 6747 (1998).

[32]Y. Liu, J. Yu, W. M. Tang, and P. T. Lai, Appl. Phys. Lett. **105**, 223503 (2014).

[33]K. Murakami, M. Rommel, V. Yanev, T. Erlbacher, A. J. Bauer, and L. Frey, J. Appl. Phys. **110**, 054104 (2014).

[34]P. Smertenko, L. Fenenko, L. Brehmer, and S. Schrader, Adv. Colloid Interface Sci. **116**, 255 (2005).

[35]O. Ya. Olikh, J. Appl. Phys. **118**, 024502 (2015).

[36]C. Acha, J. Appl. Phys. **121**, 134502 (2017).

[37]M. Lyakas, R. Zaharia, and M. Eizenberg, J. Appl. Phys. **78**, 5481 (1995).

[38]M. A. Lampert and P. Mark, *Current Injection in Solids* (Academic Press, New York, 1970).

[39]J. W. Schwede, I. Bargatin, D. C. Riley, B. E. Hardinm, S. J. Rosental, Y. Sun, F. Schmitt, P. Pianetta, R. T. Howe, Z. Shen, and N. A. Melosh, Nat. Mater. **9**, 762 (2010).

[40]M.-Y. Lu, M.-P. Lu, S.-J. You, C.-W. Chen, and Y.-J. Wang, Sci. Rep. **5**, 15123 (2015).

[41]A. K. Sharma, S. N. Singh, N. S. Bisht, H. C. Kandpal, and Z. H. Khan, Sol. Energy Mater. Sol. Cells **100**, 48 (2012).

[42]S. I. Pekar, Z. Eksp. Teor. Fiz. **10**, 1210 (1940).

[43]S. I. Pekar, Z. Eksp. Teor. Fiz. **11**, 708 (1941).